

# Prompt-NO formation revisited: detecting NCN in low and atmospheric pressure flames

R.J.H. Klein-Douwel\*, N.J. Dam and J.J. ter Meulen

Applied Molecular Physics, Institute for Molecules and Materials,  
Radboud University Nijmegen, P.O. Box 9010, 6500 GL Nijmegen, The Netherlands

## Abstract

The cyanitrene radical, NCN, is detected by laser-induced fluorescence in laminar, adiabatic, flat  $\varphi = 1.3$  methane/air flames at 200 hPa and atmospheric pressure. Laser excitation of the  $\tilde{A}^3\Pi_u(020) - \tilde{X}^3\Sigma_g^-(000)$  band at 317 nm allows off-resonant fluorescence to be detected at 326 nm. Excitation and dispersed fluorescence spectra are presented, as well as profiles of NCN and CH *versus* height above burner. Preliminary results of cavity ring-down absorption measurements are shown also.

## Introduction

Prompt NO formation in combustion processes has been relatively well understood since the early work of Fenimore [1]. The rate-limiting reaction has long been thought to be  $\text{CH} + \text{N}_2 \leftrightarrow \text{HCN} + \text{N}$ . Recently, however, it has been found that this reaction, which is spin-forbidden, has to be replaced by  $\text{CH} + \text{N}_2 \leftrightarrow \text{NCN} + \text{H}$  [2]. By now, this reaction is being incorporated in chemical mechanisms [3–5]. The importance of NCN in combustion processes has also been derived from studies on NO [6] and HCN [7].

The spectroscopy of NCN has been pioneered by Herzberg [8] and later expanded by *e.g.* Kroto *et al.* [9, 10], Smith and co-workers [11] and Beaton *et al.* [12, 13]. Its diagonal transitions [*e.g.* (000) – (000) or (020) – (020)] are much stronger than the off-diagonal ones [*e.g.* (020) – (000)]. NCN has been observed in emission of flames containing active nitrogen [14], cyanogen [15] or fluorine [16] and in comets [17, 18].

NCN has first been observed in flames by laser-induced fluorescence (LIF) by Smith [19], using a methane/air flame with fuel equivalence ratio  $\varphi = 1.3$  at 40 hPa. In that study, NCN is excited in the 327 – 329 nm range, where the signals are due to the  $\tilde{A}^3\Pi_u(000) - \tilde{X}^3\Sigma_g^-(000)$  band and (010) – (010) hot bands. The LIF wavelength of these bands is (almost) resonant with the excitation wavelength. More recently, NCN LIF has been detected in very similar flames [20, 21] (at 40 and 53 hPa, respectively) and in a shock-tube [22], using the same transitions. In [20, 22] the signal is assigned to NCN based on the excitation wavelength of 329.13 nm. Nearby OH LIF is employed in [20] to obtain semiquantitative NCN mole fractions, while use of cavity ring-down spectroscopy and spectral simulation yielded an absolute NCN concentration of  $170 \pm 90$  ppb in the flame used in [21].

## Specific objectives

Elastic light scattering is manageable at the low pressures used in [19–21], but at higher pressures, more realistic for practical combustion applications, it becomes problematic. This can be avoided by using the NCN  $\tilde{A}^3\Pi_u(020) - \tilde{X}^3\Sigma_g^-(000)$  band, as suggested in [11] (but not observed in [19]). This paper describes LIF detection of this band in flames (at 200 hPa and atmospheric pressure) and excitation and dispersed fluorescence spectra are compared to data in [11] (see also [23]). Since insufficient spectroscopic data is known for this band (in contrast to the bands used in [19–22]), results presented here must remain qualitative.

The cavity ring-down (CRD) absorption technique has the benefit, compared to the LIF technique, that absolute concentration measurements are possible, if the spectroscopic constants like absorption cross-sections are known. Unfortunately, for the  $\tilde{A}^3\Pi_u(020) - \tilde{X}^3\Sigma_g^-(000)$  band at 317 nm these are not known. Furthermore, the absorption wavelength for NCN in this region is very close to a strong OH absorption (see below), impeding spectral separation. Therefore attention has been given to the absorption of the  $\tilde{A}^3\Pi_u(000) - \tilde{X}^3\Sigma_g^-(000)$  band at 329 nm, as is used in [21]. This reference also gives an absorption cross-section for the  $\tilde{A}^3\Pi_u(000) - \tilde{X}^3\Sigma_g^-(000)$  band. Note that the NCN spectrum given in [21] is an LIF excitation spectrum.

## Experimental setup

### Burner system

The burner system is almost identical to the one described in [24]; some details are given here. The burner deck consists of a perforated plate of 30 mm diameter (0.5 mm diameter holes at 0.7 mm pitch) and the flows of methane and air are computer-controlled by mass flow controllers. The burner deck is preheated by an outer ring to compensate for heat loss of the flame to the burner deck and thermocouples are used for checking adiabaticity. The entire burner system is mounted on a

\*Corresponding author: R.Klein-Douwel@science.ru.nl  
Proceedings of the European Combustion Meeting 2009

calibrated vertical translator. The height-above-burner  $h_{ab}$  of the laser beam (derived from Rayleigh scattering) is measured with a camera system (described below). Measurements have been performed in laminar,  $\varphi = 1.3$ , methane/air flames at pressures of 200 and 1000 hPa. At the latter (atmospheric) pressure, the flame front is thinner and closer to the burner. Results are shown for a pressure of 200 hPa, unless stated otherwise.

### Laser-induced fluorescence

The  $\tilde{A}^3\Pi_u(020) - \tilde{X}^3\Sigma_g^-(000)$  band of NCN is excited at 316.970 nm [11] by frequency doubling (in a KDP crystal) the output of a Nd:YAG-pumped tunable dye-laser (Quantel YG781C10 [5 ns pulse] and Quantel TDL50, respectively) operating on a mixture of DCM and Pyridine-1 dyes dissolved in ethanol. The resulting ultraviolet laser light is focused above the burner by an  $f = 430$  mm lens and has a full-width-half-maximum (FWHM) diameter of 0.7 mm. The laser beam polarization is such, that detection of Rayleigh scattering is minimized, but it is still significant. The laser power is 50 – 100  $\mu\text{J}/\text{pulse}$ , so saturation is not expected to happen for NCN or CH, but may occur for OH (which is recorded for wavelength calibration purposes only). Since the selected NCN band is relatively weak, higher laser powers may be used while still avoiding saturation.

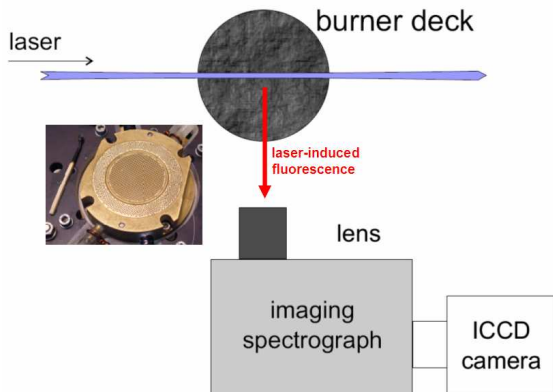


Fig. 1. Experimental setup for laser-induced fluorescence measurements.

Figure 1 shows the experimental setup for laser-induced fluorescence measurements. The LIF signal is observed at right angles to the laser beam with an intensified CCD camera (Princeton Instruments THM, 512×512 pixels, 16-bit dynamic range), which is mounted behind a spectrograph (Acton SP300i) equipped with a UV Nikkor  $f = 105$  mm,  $f/4.5$  lens. The spectrograph entrance slit is parallel to the laser beam and the burner deck. Dispersed fluorescence spectra have been taken with a 2400 grooves/mm grating, yielding a total view of about 18.8 nm in one direction of the camera image (0.037 nm/pixel). The perpendicular image direction represents spatial information (at

0.15 mm/pixel) and captures more than the entire width of the flame. In order to increase the signal/noise ratio, however, spectra have been recorded while binning together pixels in the spatial direction over almost the entire width of the flame. In this way dispersed fluorescence spectra could be recorded rapidly and continuously while the laser excitation wavelength was scanned slowly, yielding two-dimensional excitation – dispersion spectra.

### Cavity ring-down

Figure 2 shows the low pressure cavity ring-down setup. Between the mirrors and the burner small diameter tubes are fitted, which are continuously flushed with a slow flow of nitrogen, in order to remove water vapour and possible OH between the mirrors and the flame and to limit the absorption path to approximately the width of the flame.

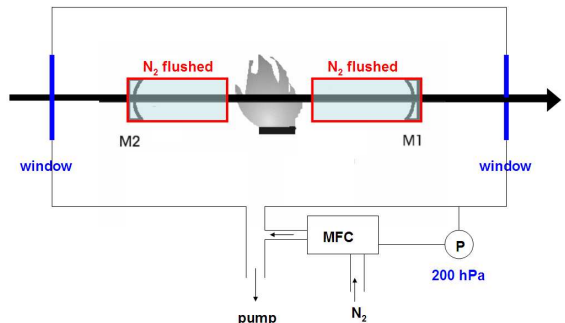


Fig. 2. Low pressure cavity ring-down setup.

## Results and discussion

### Laser-induced fluorescence

Figure 3 presents an example of an LIF excitation – dispersion spectrum, in which 100 laser shots are integrated per dispersed fluorescence spectrum. From these spectra, separate excitation and dispersed fluorescence spectra are easily obtained. The spectrograph – camera combination is also used to record the position of the flame front, using  $\text{CH}^*$  chemiluminescence as a marker.

LIF signal of NCN and spectrally nearby transitions of OH (A – X system) and CH (C – X system) are recognizable in Fig. 3 and the wavelengths of OH and CH lines are used for accurate spectral calibration of both wavelength axes using LIFBASE [25]. Employing an excitation – dispersion spectrum, as displayed in Fig. 3, shows that in case of nearly equal excitation wavelengths, species can still be identified and spectrally separated by their dispersed fluorescence wavelengths. Reference measurements of CH LIF are performed by exciting the  $\text{P}_1(9)(0,0)$  C – X transition at 316.943 nm. The population of the lower level of this transition is relatively insensitive to temperature variations in the range encountered in this flame, so that its intensity is a coarse measure of the local CH density.

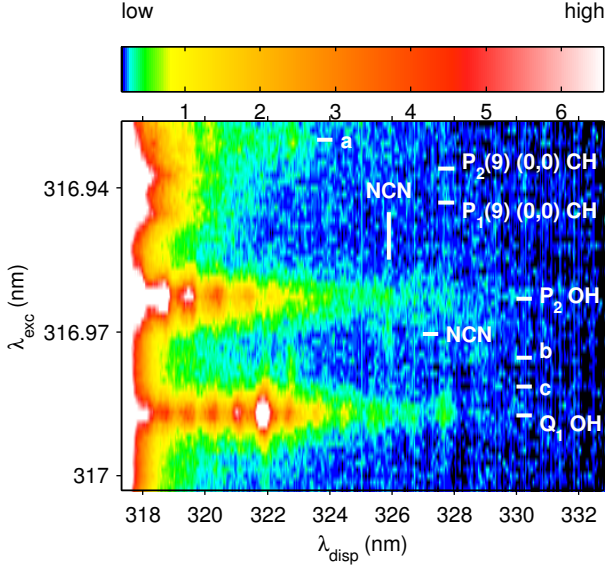


Fig. 3. Excitation – dispersion spectrum, recorded at the flame front. LIF features originating from NCN, CH and OH are identified: 'NCN' and 'P<sub>2</sub>/Q<sub>1</sub> OH' are explained in Fig. 4; 'a' = P<sub>12</sub>(15) (0,0) OH, 'b/c' = Q<sub>1</sub>/Q<sub>2</sub>(21) (1,1) CH ( $\lambda_{disp} = 322.7$  nm for 'a/b/c'). Low intensities are enhanced in a non-linear way (detector saturated near laser wavelength).

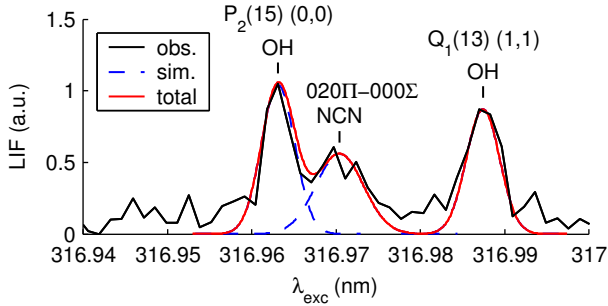


Fig. 4. Excitation spectrum of the NCN  $\tilde{A}^3\Pi_u(020) - \tilde{X}^3\Sigma_g^-(000)$  band head.

An excitation spectrum of the  $\tilde{A} - \tilde{X}$  (020) – (000) band head of NCN at 316.970 nm [11], derived from Fig. 3, is presented in Fig. 4. Only fluorescence between 325.67 and 326.00 nm is selected for extracting the excitation spectrum. The P<sub>2</sub>(15) (0,0) and Q<sub>1</sub>(13) (1,1) transitions of OH are detected as well. The spectral lines are simulated by gaussian curves. For OH a FWHM of 0.0047 nm is used (consistent with nearby OH lines not shown here), for NCN a FWHM of 0.0067 nm is used. It must be noted that at  $\lambda_{exc} = 316.966$  nm both the O<sub>12</sub>(4) (1,1) transition of OH and the O<sub>12</sub>(5) (0,0) transition of CH can be excited, but the fluorescence of both these two lines is blue-shifted relative to the excitation wavelength and therefore not present in the excitation spectrum in Fig. 4.

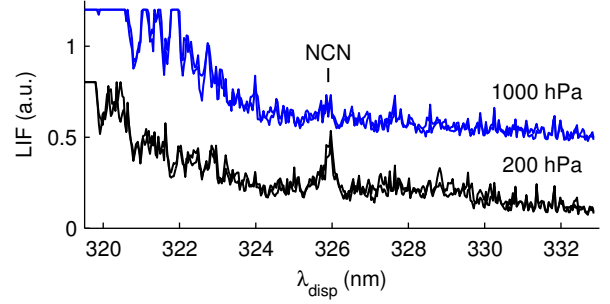


Fig. 5. Spectra of dispersed fluorescence following excitation of the  $\tilde{A} - \tilde{X}$  (020) – (000) band head (2 spectra at each pressure, vertical offset between pressures for clarity; detector saturated for  $\lambda_{disp} \leq 320$  nm).

Dispersed fluorescence spectra are recorded at the flame front by integrating 1800 laser shots at a fixed  $\lambda_{exc} = 316.970$  nm. Figure 5 shows the results in the 200 hPa and atmospheric pressure flames. Two separately recorded spectra are shown for each pressure, indicating good reproducibility. The NCN fluorescence at 325.90 nm most likely originates from the (020) – (020) band [11] and is clearly visible in the 200 hPa spectrum and still present (but harder to see) in the 1000 hPa spectrum. Both the excitation and maximum fluorescence wavelengths correspond very well to literature values [11], thereby confirming the assignment of these signals as belonging to NCN. Other NCN transitions in the region  $315 \leq \lambda_{exc} \leq 320$  nm (the weaker features in [11]) could not be detected in the flame.

Use of the current detection scheme, which has maximum fluorescence signal at a wavelength clearly separated from the excitation wavelength, allows detection of NCN under (flame) conditions where elastic laser light scattering may be too large for resonant detection, that is at higher pressures or very close to a surface. These last two conditions both apply to the measurements at atmospheric pressure presented here, but in this case LIF of NCN can still be detected at the flame front because a spectrograph is used.

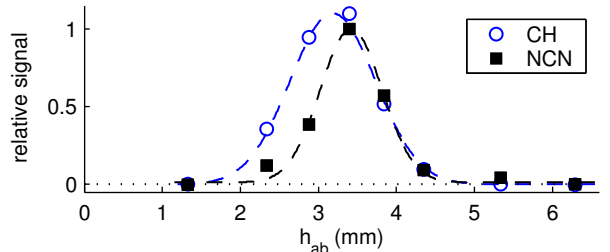


Fig. 6. NCN and CH LIF signal *versus*  $h_{ab}$  in the 200 hPa flame. Gaussian fits guide the eye.

The thickness of the flame front and its separation from the burner allow dispersed fluorescence spectra of NCN to be recorded *versus*  $h_{ab}$  at 200 hPa. To this end, a linear background is fit and the remaining net signal

between 325.71 and 326.07 nm is integrated. A similar procedure is followed for dispersed fluorescence spectra of CH after exciting the  $P_1(9)(0,0)$  C - X transition. In this case the net signal of the Q branch is integrated between 313.87 and 314.79 nm, with integration of 200 laser shots per spectrum being sufficient. The resulting variations of net NCN and CH signals with  $h_{ab}$  are shown in Fig. 6.

From this data it is clear that the NCN signal peaks somewhat higher above the burner than CH, that the NCN distribution is somewhat narrower than that of CH and also that the presence of NCN is limited to the flame front. These results are similar to those observed in [19–21]. In those studies the FWHM of the NCN distribution is slightly larger than 2 mm (at  $\leq 53$  hPa), whereas here it is about 0.9 mm at 200 hPa. This difference is caused by the higher pressure. The  $h_{ab}$  of maximum NCN signal presented here differs from that in [19–21], but apart from pressure effects this may be due to different burner/flame conditions in those studies.

### Cavity ring-down

Figure 7 shows a preliminary result of an experimental CRD absorption spectrum in the region where NCN absorption is expected. Simulations of OH (A - X system) and CH (C - X system) absorption (from LIFBASE [25]) and NCN absorption ( $\tilde{A}^3\Pi_u(000) - \tilde{X}^3\Sigma_g^-(000)$  band; from PGOPHER [26]) are given as well. Comparison to the experimental spectrum shows that it is difficult to separate the possibly measured NCN absorption from that of OH. There is reasonable agreement between the measured and simulated spectra, except for the peak at 329.08 nm. Therefore further investigations are required.

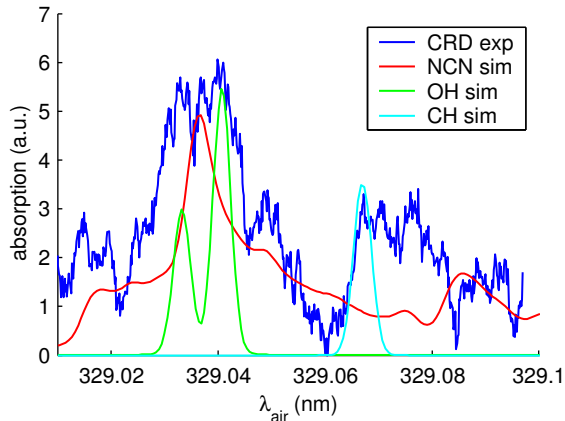


Fig. 7. CRD absorption spectrum recorded at the flame front, compared to simulations of OH, CH and NCN absorption (scaled individually for each species). The OH transitions are the  $P_{12}(4)$  and  $P_2(4)$  (3,3) lines, the CH transition is the  $O_{12}(29)$  (0,0) line. Wavelengths are given in air.

## Conclusions

In summary, clear LIF spectra of the NCN  $\tilde{A}^3\Pi_u(020) - \tilde{X}^3\Sigma_g^-(000)$  band have been recorded in a  $\varphi = 1.3$  methane/air flame at both 200 hPa and atmospheric pressure. This extends NCN measurements to higher pressures than reported in earlier literature [19–21]. Using the off-resonant excitation – detection scheme presented here ( $\lambda_{exc} = 316.970$  nm and  $\lambda_{disp} = 325.90$  nm) allows unambiguous detection of NCN [11]. It also allows NCN LIF to be measured in situations with more laser light scattering, either from Rayleigh scattering at higher pressures or reflections off surfaces. Variation of NCN signal (with respect to that of CH) with height above burner, as observed here at 200 hPa, is similar to that presented in [19–21]. CRD absorption measurements need more work.

## Acknowledgments

Discussions with A.A. Konnov (Vrije Universiteit Brussel and Technische Universiteit Eindhoven) are gratefully acknowledged, as is technical support from L. Gerritsen and A.P. van Vliet and financial support from the Technology Foundation STW. Discussions with C.M. Western (University of Bristol), who supplied the PGOPHER [26] data file for the NCN absorption simulation, are also gratefully acknowledged.

## References

1. C. P. Fenimore, Proc. Combust. Inst. **13**, 373 (1971).
2. L. V. Moskaleva and M. C. Lin, Proc. Combust. Inst. **28**, 2393 (2000).
3. A. El bakali, L. Pillier, P. Desgroux, B. Lefort, L. Gasnot, J. F. Pauwels, and I. da Costa, Fuel **85**, 896 (2006).
4. J. A. Sutton and J. W. Fleming, Combust. Flame **154**, 630 (2008).
5. A. A. Konnov, Combust. Flame (2008, submitted).
6. B. A. Williams and J. W. Fleming, Proc. Combust. Inst. **31**, 1109 (2007).
7. S. Gersen, A. V. Mokhov, and H. B. Levinsky, Combust. Flame **155**, 267 (2008).
8. G. Herzberg and D. N. Travis, Can. J. Phys. **42**, 1658 (1964).
9. H. W. Kroto, J. Chem. Phys. **44**, 831 (1966).
10. H. W. Kroto, T. F. Morgan, and H. H. Sheena, Trans. Faraday Soc. **66**, 2237 (1970).
11. G. P. Smith, R. A. Copeland, and D. R. Crosley, J. Chem. Phys. **91**, 1987 (1989).
12. S. A. Beaton, Y. Ito, and J. M. Brown, J. Mol. Spectrosc. **178**, 99 (1996).
13. S. A. Beaton and J. M. Brown, J. Mol. Spectrosc. **183**, 347 (1997).
14. K. R. Jennings and J. W. Linnett, Trans. Faraday Soc. **56**, 1737 (1960).
15. E. M. Bulewicz, Proc. Combust. Inst. **12**, 957 (1969).
16. M. Vanpee, P. Vidaud, and K. D. Cashin, Combust. Flame **23**, 227 (1974).

17. C. R. O'Dell, C. O. Miller, A. L. Cochran, W. D. Cochran, C. B. Opal, and E. S. Barker, *Astrophys. J.* **368**, 616 (1991).
18. J. H. Valk, C. R. O'Dell, A. L. Cochran, W. D. Cochran, C. B. Opal, and E. S. Barker, *Astrophys. J.* **388**, 621 (1992).
19. G. P. Smith, *Chem. Phys. Lett.* **367**, 541 (2003).
20. J. A. Sutton, B. A. Williams, and J. W. Fleming, *Combust. Flame* **153**, 465 (2008).
21. N. Lamoureux, X. Mercier, C. Western, J. F. Pauwels, and P. Desgroux, *Proc. Combust. Inst.* **32**, 937 (2009).
22. V. Vasudevan, R. K. Hanson, C. T. Bowman, D. M. Golden, and D. F. Davidson, *J. Phys. Chem. A* **111**, 11818 (2007).
23. R. J. H. Klein-Douwel, N. J. Dam, and J. J. ter Meulen, *Opt. Lett.* **33**, 2620 (2008).
24. K. J. Bosschaart and L. P. H. de Goeij, *Combust. Flame* **132**, 170 (2003).
25. J. Luque and D. R. Crosley, "LIFBASE: Database and spectral simulation (version 2.0.60, 2008)", Tech. rep., SRI International (1999). Report MP 99-009.
26. "PGOPHER, a Program for Simulating Rotational Structure", C.M. Western, University of Bristol, <http://pgopher.chm.bris.ac.uk> (2009).